Experimental and Numerical Investigation of Mode Veering in a Stressed Structure

J. L. du Bois, S. Adhikari and N. A. J. Lieven

Department of Aerospace Engineering, University of Bristol, Queens Building, University Walk, Bristol BS8 1TR (U.K.)

ABSTRACT

The manifestation of mode veering in structural dynamic problems has been the subject of much debate in recent years. Initially regarded as an anomolly occurring predominantly as a result of numerical discretisation errors, it is now recognised as a phenomenon occurring in a wide range of exact analytical solutions. Myriad theoretical studies have explored the characteristics of the behaviour but despite this, supporting experimental data is scarce. A numerical and experimental investigation of mode veering is undertaken here. Structural loading is used to induce striss-stiffening effects in a redundant truss. Geometric nonlinearities are included in a static FE analysis to obtain a tangent stiffness, which is then used in a linear dynamic solution. The eigenvalues and eigenvectors are compared to the experimental data in the vicinity of a mode veering, where the behaviour of the real structure is found to correspond well with the theoretical observations. Practical implications of real-world mode veering are discussed.

Nomenclature

λ_i	i^{th} eigenvalue
ϕ_i	i^{th} eigenvector (mass normalised)
θ	structural parameter
ε	perturbation to structural parameter
ε_x, ε_y	axial and transverse elemental strain
A	cross-sectional area
CF_{ij}	coupling factor between modes i and j
E	Young's modulus
K_E	elastic stiffness matrix
K_G	geometric stiffness matrix
K_T	tangent stiffness matrix
L	length
u, v	axial and transverse beam displacements
$\mathbf{K}$	stiffness matrix
$\mathbf{M}$	mass matrix

1 INTRODUCTION

Changes in dynamic response through structural parameter variation are routinely characterised in plots of the eigenvalue loci over the parameter range of interest. It is common for adjacent loci to follow intersecting trajectories. For self-adjoint eigenproblems, as encountered in general structural dynamic work, the loci in these regions will either be seen to cross or veer suddenly away from each other.

Since the first theoretical observations of mode veering [1–6], the combination of a lack of experimental evidence and discrepancies between results from different numerical and analytical techniques [5, 6] has prompted debate about the existence of veering in practical systems. It is now well established that although veering can be an aberration produced by spatial discretisation and poor damping models (see [6, 7]), there exist systems for which exact analytical solutions exhibit the phenomenon [8]. The following sections will summarise the theoretical characteristics of mode veering and go on to present finite element (FE) and experimental results to support these ideas.

The structure used to demonstrate the behaviour is a redundant truss. The parameter varied is the internal pre-stress, which induces an effect known as *stress stiffening*. This is a manifestation of geometric nonlinearity, whereby the transverse stiffness of a beam or shell is affected by applied axial or membrane loads. This has been used for millennia in stringed musical instruments, where the pitch is varied by tensioning the strings. It is also illustrated by the well-known Euler buckling instability, a special case of the generalised result provided by Warburton [9]. Slender structures are designed primarily to carry only axial loading. As such, the effect of stress stiffening on static displacement is usually minimal. The dynamic response of the structure, however, can be greatly influenced by the change in transverse stiffness. This was exploited as far back as 1936, when Stephens [10] explained how the natural frequencies of a structure can be used to determine the load carried in its members.

Internal pre-stressing of a framed structure will cause some members to experience compression while others are placed in tension. The contrasting effects on stiffness of the members creates a structure with both rising and falling natural frequencies, ideal for studying the interactions of the modes as they converge. The advantage of using a continuously adjustable parameter such as pre-stress is also evident when the small range of parameter values over which veering occurs is considered.

2 A BRIEF REVIEW OF MODE VEERING

Mode veering is characterised by the sharp transition of two convering eigenvalue loci to new trajectories. After veering, each locus continues on the path previously followed by the other. As well as the rapid change in eigenvalue sensitivities, it has long been known that the mode shapes undergo violent changes as they veer, described elegantly by Leissa [6]: "figuratively speaking, a dragonfly one instant, a butterfly the next, and something indescribable in between." The modes effectively swap with each other, each one taking on the characteristics of the other. It is for this reason that rapid mode veering in experimental results will often go undetected: If data is only recorded for parameter values either side of the veering region, and not for the narrow band within the veering region, it is almost indistinguishable from a crossing.

Modes in symmetric structures are always symmetric or antisymmetric with respect to that symmetry. Webster [11] and Petyt and Fleischer [5] both note that a symmetric mode's frequency locus will pass through that of an antisymmetric mode, with the two modes coexisting at the same frequency, yet two symmetric or two antisymmetric modes will generally veer. Any imperfections will remove the symmetry, producing weak modal coupling so that all proximate loci will tend to exibit veering.

Some efforts have been made to establish and define the conditions under which veering occurs. Perkins and Mote [8] derive perturbation expressions for the eigenvalues of two proximate modes and determine "coupling factors" to quantify the eigenfunction coupling. For a symmetric, self-adjoint, matrix eigenproblem the coupling factors are given by

$$CF_{ij} = \left[\phi_i^T \left(\frac{\partial \mathbf{K}}{\partial \theta} - \lambda_i \frac{\partial \mathbf{M}}{\partial \theta} \right) \phi_j \right]^2 \tag{1}$$

where θ is the parameter, ϕ_i and ϕ_j are the two eigenvectors, λ_i is the i^{th} eigenvalue and $\mathbf{M}$ and $\mathbf{K}$ are the system mass and stiffness matrices. It is assumed that the two eigenvalues are close to each other and distant from other eigenvalues, meeting the criterion

$$|\lambda_i - \lambda_j| \leq \varepsilon \{ \min_{r,s \neq i,j} |\lambda_r - \lambda_s| \} \tag{2}$$

where ε is a perturbation to the parameter, θ, of the same order of magnitude as the veering region. In this case the behaviour of the loci depends on the coupling factors: without coupling the loci are locally independent and free to cross;

otherwise, for self-adjoint problems, the coupling factors will be positive and the curves will veer away from each other. This provides a useful tool for ascertaining whether two modes will cross or veer and how abrupt the changeover will be. Small coupling factors correspond with rapid veering, while large coupling factors represent more gentle transformations.

Another useful characterisation is to examine the eigenvector rotations of the two modes, responsible for their aesthetically bizarre transformatons. Balmès [12] expressed system properties for a three degree of freedom lumped-mass system in terms of two eigenvalue perturbations and a rotation angle, θ, and demonstrated that as two of the modes went through a veering region the eigenvectors both rotate in their plane by the angle θ. It can be demonstrated that as any two modes veer, provided their proximity to each other is much greater than to any other modes, they will remain roughly in the same plane, or subspace, and both rotate by the same angle in the normal coordinate system. The total angle of rotation undergone throughout a veering is related to the severity of the veering. The more violent the veering, the greater the rotation, tending to a maximum total of 90° as the coupling factors go to zero and the veering becomes a crossing. This means that the more rapid the veering, the closer the resemblance between the pre-veering mode shapes and the swapped post-veering mode shapes.

3 REDUNDANT TRUSS EXAMPLE

3.1 Experimental Setup

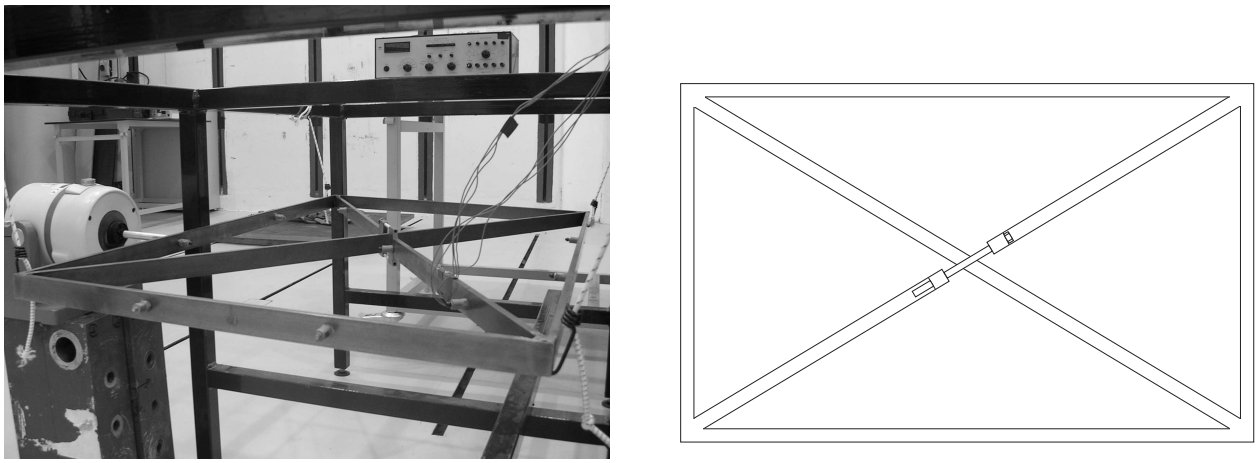

(a) Experimental setup

(b) Schematic layout

Figure 1: The redundant frame with tightening mechanism in one of the diagonal members. The two diagonals are not connected where they cross. The corner joints are rigidly welded.

The experimental arrangement can be seen in Fig. 1(a). A redundant structure was designed in the form of a cross-braced rectangle, shown schematically in Fig. 1(b). The corner joints are welded, as this connectivity introduces the least uncertainty to the structure. Two bolts in one of the diagonal members pass either side of the other cross-beam so there is no contact between the two members. When the bolts are tightened, they shorten that member, resulting in a load transmitted throughout the structure, with the diagonal members in tension and the outside members in compression. To simplify the FE analysis the beams are arranged to behave as a 2-dimensional system. The second moment of area of each beam in the plane of the structure is far smaller than that perpendicular to the plane so the vibration modes out of plane will occur at much higher frequencies than those in plane. All of the beam centrelines lie in one plane to avoid coupling between in-plane and out-of-plane modes.

In light of the discussion in section 2 it is relevant to note that the structure does not have reflectional symmetry due to the considerably lower stiffness of the tensioning mechanism compared to that of the solid cross-member. It does, however, have rotational symmetry.

The framework is suspended by rubber bands to approximate free vibration conditions and fourteen accelerometers are attached. In order to control the loading of the structure, strain gauges are mounted on top and bottom of the adjustable member. By balancing the two gauges it is possible to ensure that no bending moment is induced in the structure by uneven tightening of the two tensioning bolts. LMS spectral aquisition software [13] is used with a single shaker to supply broadband excitation to the structure and obtain the FRFs and modal response. The modal characteristics are identified using a least squares complex exponential parameter estimation technique in the time domain with multiple degrees of freedom. The mode shapes are simplified to real approximations and this is justified by noting that the damping will be very low throughout this structure and the complex parts of the mode vectors will be negligible. The modes are expanded using a reversed Guyan reduction technique [14, pp.68-69] and mode correlation between load cases is automated using a MAC-based algorithm [14, pp.56-57].

3.2 Finite Element Model and Results

The FE model uses 6 two-dimensional Euler-Bernoulli beam elements to represent each member. The tightening mechanism is represented by a further 3 elements. The static loading is modelled by removing the coupling between the bolts and the frame at one end of the mechanism. The free end of the frame is fully constrained and the free end of the bolts is constrained in the transverse and rotational degrees of freedom (DOFs), leaving the axial DOF unconstrained. A load is then applied axially to this end. Once the static solution is obtained, the two free ends can be rigidly joined again and the constraints removed to obtain the free dynamic response.

3.2.1 STRESS STIFFENING

Geometric nonlinearities are characterised on a load-displacement graph by the changing gradient of the curve. The stiffness at a given point is represented by the tangent to the curve and referred to as the *tangent stiffness*. The approach adopted here is to first use a nonlinear static analysis to determine the tangent stiffness for a given load case. Then, assuming small dynamic loads and displacements, the tangent stiffness is used to obtain a linear dynamic solution for this load case.

Geometric nonlinearity is commonly included in static structural problems [15], and is generally split into two categories: stress stiffening and large deformation. In finite element analyses, the latter is usually subcategorised further into large elemental rotations and large elemental strains. Stress stiffening is the most important factor for lower loads and small deformations, where its effect on dynamic response is belied by its relative insignificance in static solutions. As structural deformation increases it becomes necessary to take elemental rotations into account, but the further complication of large elemental strain is easily avoided in simple models through refinement of the spatial discretisation. It is common to derive a geometric stiffness matrix based on axial load which, when added to the elastic stiffness matrix K_E, gives the tangent stiffness:

$$K_T = K_E + K_G$$

The elements used in this analysis are simple two-dimensional Euler-Bernoulli beam elements [16, p.81] with six degrees of freedom: two translational and one rotational at each end. Jennings [17] uses a series of transformations to include both stress stiffening and large deformation effects in the stiffness matrix. He derives an exact solution and a computationally efficient approximation based on second order expansions of the axial strain term. Using his second order approximation a geometric stiffness matrix can be formed in terms of the axial and transverse end displacements:

$$K_G = \frac{EA}{L}\begin{bmatrix} 0 & \varepsilon_y & 0 & 0 & -\varepsilon_y & 0 \\ \varepsilon_y & \left(\varepsilon_x + \frac{3}{2}\varepsilon_y^2\right) & 0 & -\varepsilon_y & -\left(\varepsilon_x + \frac{3}{2}\varepsilon_y^2\right) & 0 \\ 0 & 0 & 0 & 0 & 0 & 0 \\ 0 & -\varepsilon_y & 0 & 0 & \varepsilon_y & 0 \\ -\varepsilon_y & -\left(\varepsilon_x + \frac{3}{2}\varepsilon_y^2\right) & 0 & \varepsilon_y & \left(\varepsilon_x + \frac{3}{2}\varepsilon_y^2\right) & 0 \\ 0 & 0 & 0 & 0 & 0 & 0 \end{bmatrix} \quad \text{where } \begin{matrix} \varepsilon_x = \frac{u_2 - u_1}{L} \\ \varepsilon_y = \frac{v_2 - v_1}{L} \end{matrix} \tag{3}$$

and u and v are the axial and transverse displacements, E is the Youngs Modulus, A the cross-sectional area and L the

length of the beam.

Closed form solutions for general nonlinear structural problems are rare and iterative techniques are usually employed. A common method, employed here, is to calculate the displacement at small load intervals using linear theory, evaluating a new tangent stiffness at each step. Newton-Raphson iterations [18, pp.277-280] are employed to reduce the residual force at each load increment.

As with the experimental data, modes are correlated between load steps using a MAC-based algorithm.

3.2.2 RESULTS

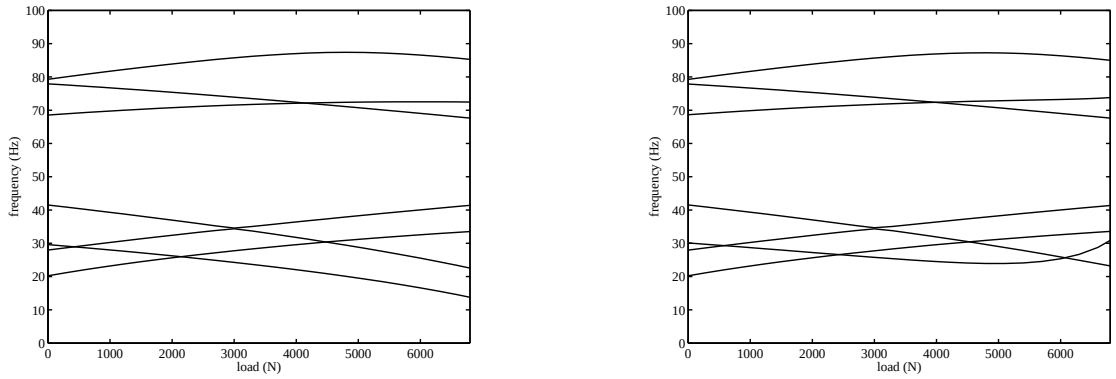

(a) Initial FE model

(b) Perturbed FE model

Figure 2: Eigenfrequency loci plotted with varying load from finite element data. A small initial perturbation of the side members results in significantly different behaviour close to the buckling load.

The eigenfrequency loci for the initial FE model are plotted in Fig. 2(a) with load steps of 300N. The FE model was taken close to buckling at 6800N and it was found that the eigenfrequiency loci near buckling are very sensitive to the initial configuration. As an example, Fig. 2(b) shows the results for the same model run with an initial transverse curvature in the long outside members in the form of a half sine wave. The initial displacement of the beam centres is just 0.185% of the member length but produces a marked change in the dynamic behaviour close to buckling. This is attributed to the higher failure load of the ideal structure compared with the perturbed model. The ideal structure deforms linearly before suddenly buckling; in contrast, the onset of buckling begins earlier and more gradually in the perturbed structure.

The loci appear to cross in several places. The point where modes 5 and 6 meet will be examined in detail. Their mode shapes are illustrated in Fig. 3 where it can be seen that mode 5 has 'even' rotational symmetry and mode 6 has 'odd' rotational symmetry. They are therefore expected to cross rather than veer, and this is seen to be the case in Fig. 4(a). In a practical structure, perfect symmetry can not be achieved, so an arbitrary imperfection is introduced to the FE model. This takes the form of a 1% increase in the cross sectional area of two outside members, affecting the calculation of the mass and axial stiffness (but not the transverse or bending stiffness). This is seen in Fig. 4(b) to produce weak coupling between the two modes and cause them to veer instead of crossing. The mode shapes are shown at several stages throughout the veering in Fig. 5(a). As expected, after veering each mode takes on the form of the other through a smooth rotation of the eigenvectors, demonstrated in Fig. 7(a). It's interesting to note that the rotation is not through a full 90°, so the mode shapes are slightly different from those present before veering. Also, after veering, mode 6 is roughly 180° out of alignment with mode 5 before the veering:

$$\phi_6|_{post-veering} \approx -\phi_5|_{pre-veering}$$

Ordinarily this is of little interest as the scaling of the mode shapes is arbitrary so positive and negative modeshapes are equivalent but with mode veering it is important as it is indicative of which direction the eigenvectors have rotated. This in turn reflects the variation of the dynamic response throughout veering. The significance of this in terms of the *overall*

response is dependent upon the proximity of the loci and thus the severity of the veering. When the eigenvalues are very close, only the subspace occupied by the two vectors is relevant to the total response, and this remains almost constant throughout veering, regardless of the vector orientations within that subspace. This is recognised by Balmès [12], and further discussion of system response with regard to proximate eigenvalues is undertaken by Igusa [19]. If the veering is more gradual and the loci further seperated then their rotation becomes more relevant in terms of overall response, but the behaviour is then closer to normal eigenstructure variation and can not be described so well by veering characteristics and assumptions.

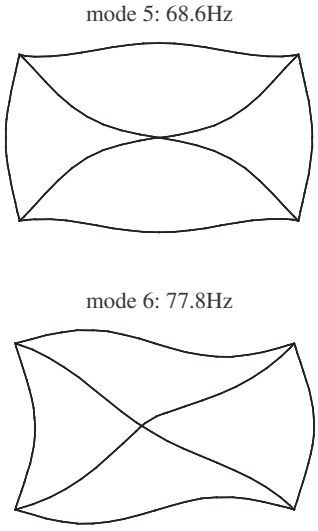

Figure 3: The fifth and sixth vibration modes of the unloaded frame

3.3 Experimental Results

The structure was tensioned, tightening the bolts incrementally by hand until the point was reached where further tightening produced little increase in the strain measurements and the structure was deemed to have buckled. Comparing the observed eigenfrequency loci from Fig. 6(a) with the initial FE model in Fig. 2(a), the two graphs clearly follow the same trends for low loads but differences emerge as the buckling load is approached. It was noted during the experiment that the buckling mode closely resembled that of the perturbed structure and, accordingly, the experimental eigenfrequencies correspond well with those in Fig. 2(b).

Focusing again on the fifth and sixth modes, close examination of the curves in Fig. 6(b) reveals unequivocally that the loci for these two modes veer away from each other. Comparing the experimental results with those for the FE model, it is found that the veering is much more gradual than in the analytical solution, occuring over a greater range of loading and with a greater seperation of the loci at their closest point.

The expanded mode shapes captured from the experiment are seen in Fig. 5(b) to match very closely those produced in the numerical model, although not at the same loads. A further discrepancy lies in the transformation of the modes. This is most obvious for the third (middle) set of mode shapes in Fig. 5, where the 5th analytical mode corresponds to the 6th experimental mode and vice versa. A clearer picture of this behaviour is obtained by comparing the experimental vector rotations with the FE rotations in Fig. 7, where it can be seen that the vectors rotate in the opposite direction. This highlights the relevance of the sign of the eigenvectors, as discussed earlier. The direction and rate of eigenvector rotation is governed by the coupling between the two modes, in this case the asymmetry of the structure. It is clear in

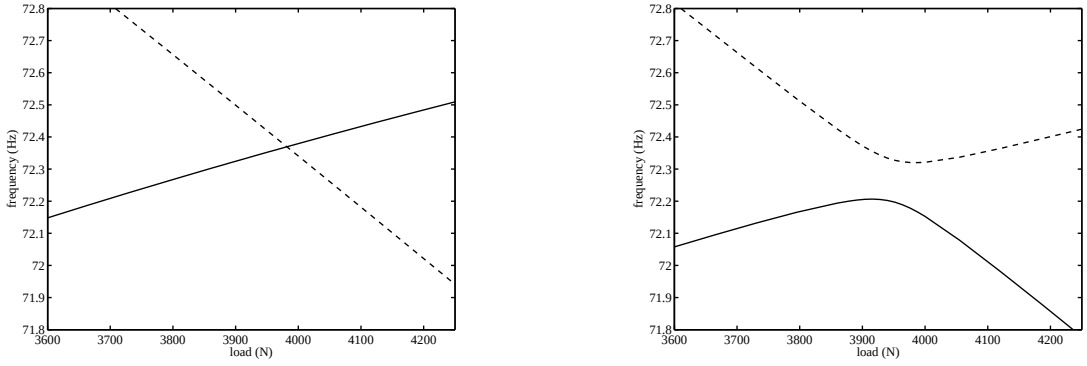

(a) Symmetric model exhibits crossing

(b) Asymmetric model exhibits veering

Figure 4: Close examination of the interaction between modes 5 (–) and 6 (- -) in the symmetric and asymmetric FE models.

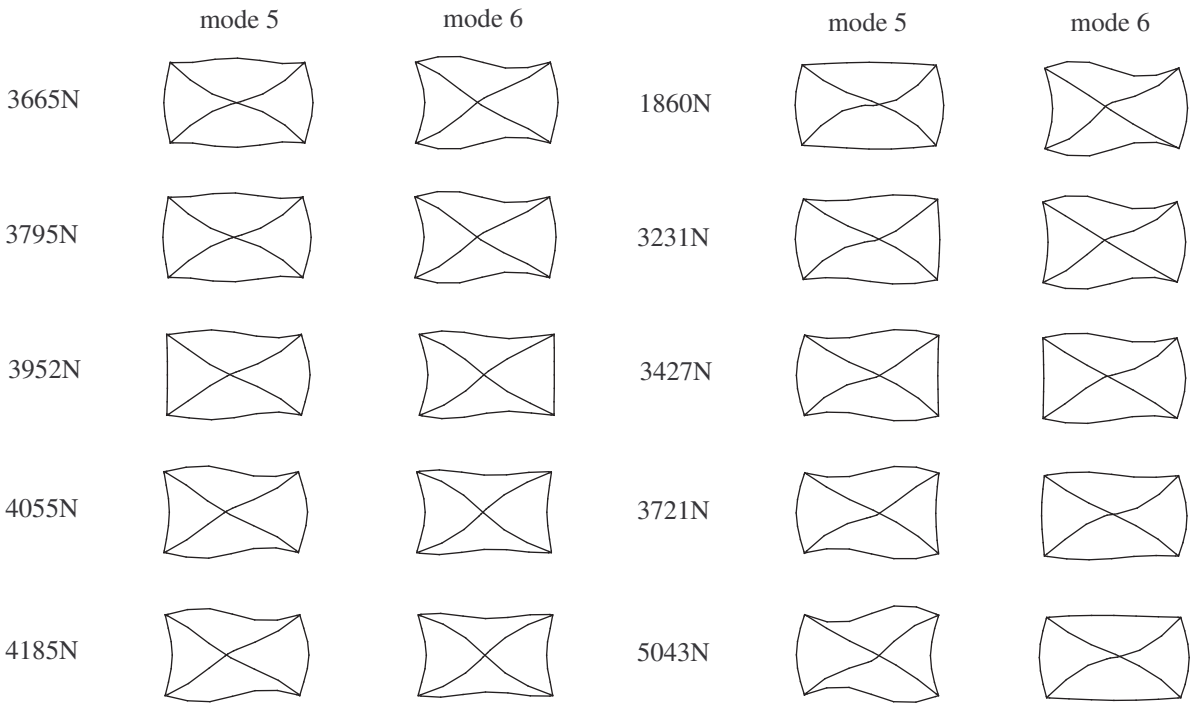

(a) FE Model

(b) Experimental Results

Figure 5: Variation of mode shapes as modes 5 and 6 approach each other and veer away. After veering mode 5 takes on the original form of mode 6 and vice versa. One mode shape is always inverted after veering.

this example that although the veering bears similarity to that of the FE model (as would *any* veering involving these two modes), the arbitrary asymmetry introduced does not match that of the actual structure. An updated model is needed, based on appropriate parameters, to match the rate and direction of the eigenvector transformations. It is possible that the eigenvector rotation could form a useful part of the objective function in an updating algorithm, particularly as it is very sensitve to small parameter changes.

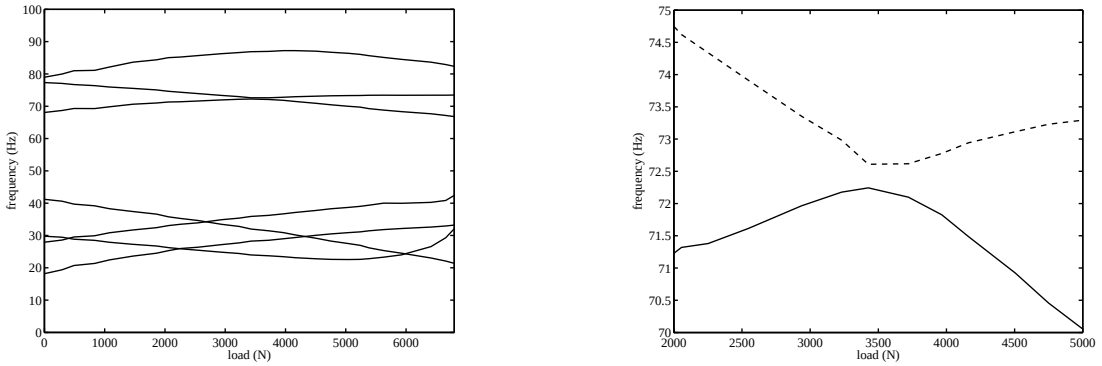

(a) Full results

(b) Close examination of the fifth (–) and sixth (- -) modes in the veering region

Figure 6: Experimental eigenfrequency loci plotted with varying load.

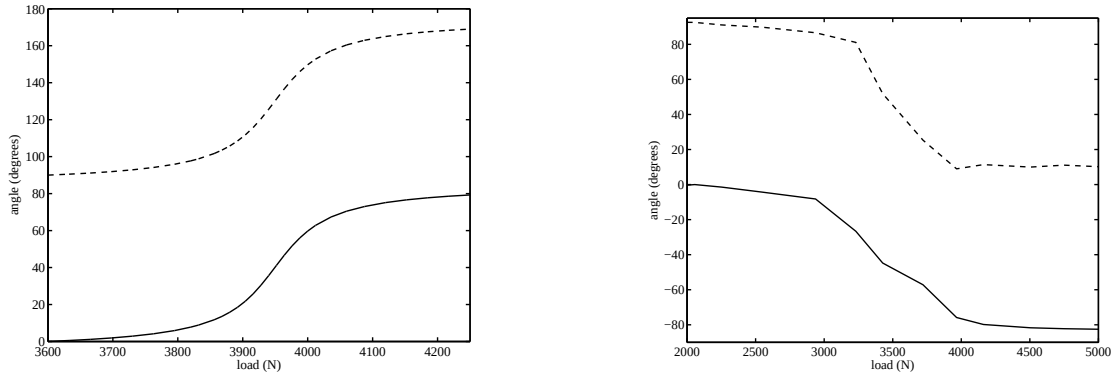

(a) FE data (b) Experimental results

Figure 7: The rotation of the 5th (–) and 6th (- -) eigenvectors in the normal coordinate system relative to the initial orientation of mode 5.

4 CONCLUSION

Mode veering is now established as a physical phenomenon occurring in real structures. The experimental results presented here confirm the veering behaviour of a real system to correspond with that predicted by finite element modelling. Applications of mode veering in response suppression are limited, as strong veering occurs only when the eigenvalues are extremely close, and in these circumstances the system response is generally affected very little by the presence of veering. An understanding of veering and the sensitive parameter dependence in these regions will, however, be necessary whenever proximate modes are studied, in both analytical and experimental situations. In addition to its general use this will be particularly relevant to, and may even find specific application in, control systems and model updating algorithms.

REFERENCES

[1] **Warburton G. B.**, *The Vibration of Rectangular Plates*, Proceedings of the Institute of Mechanical Engineers, Volume 168, pp.371-381, 1954

[2] **Mindlin R. D. and Deresiewicz H.**, *Thickness-Shear and Flexural Vibrations of a Circular Disk*, Journal of Applied Physics, Volume 25, pp.1329-1332, 1954

[3] **Claassen R. W. and Thorne C. J.**, *Vibrations of Thin Rectangular Isotropic Plates*, Journal of Applied Mechanics, Volume 28, pp.304-305, 1961

[4] **Claassen R. W. and Thorne C. J.**, *Vibrations of a Rectangular Cantilever Plate*, Journal of the Aerospace Sciences, Volume 29, No 11, pp.1300-1305, 1962

[5] **Petyt M. and Fleisxer C. C.**, *Free Vibration of a Curved Beam*, Journal of Sound and Vibration, Volume 18, No 1, pp.17-30, 1971

[6] **Leissa A. W.**, *On a Curve Veering Aberration*, Journal of Applied Mathematics and Physics (ZAMP), Volume 25, pp.99-111, 1974

[7] **Woodhouse J.**, *On the synthesis of guitar plucks*, Acta Acustica united with Acustica, Volume 90, pp.928-944, 2004

[8] **Perkins N. C. and Mote, Jr., C. D.**, *Comments on Curve Veering in Eigenvalue Problems*, Journal of Sound and Vibration, Volume 106, Issue 3, pp.451-463, 1986

[9] **Warburton G. B.**, *The Dynamical Behaviour of Structures (2nd Edition)*, Pergamon Press, 1976, ISBN 0-08-020364-7

[10] **Stephens B. C.**, *Natural Vibration Frequencies of Structural Members as an Indication of End Fixity and Magnitude of Stress*, Journal of the Aeronautical Sciences, Vol. 4, pp 54-56, 1936

[11] **Webster J.J.**, *Free vibrations of rectangular curved panels*, International Journal of Mechanical Science, Volume 10, pp.571-582, 1968

[12] **Balmès E.**, *High Modal Density, Curve Veering, Localization: A Different Perspective on the Structural Response*, Journal of Sound and Vibration, Volume 161, No 2, pp. 358-363, 1993

[13] **LMS Test Lab Spectral Aquisition User Manual, Rev 5A**, LMS International, Interleuvenlaan 68, B-3001 Leuven, Belgium, 2004

[14] **Friswell M. I. and Mottershead J. E.**, *Finite Element Model Updating in Structural Dynamics*, Kluwer Academic Publishers, 1995, ISBN 0-7923-3431-0

[15] **Crocombe A. D.**, *How to Tackle Nonlinear Finite Element Analysis*, NAFEMS, Glasgow, 2001

[16] **Przemieniecki J. S.**, *Theory of Matrix Structural Analysis*, McGraw-Hill, Inc., 1968, ISBN 07-050904-2

[17] **Jennings A.**, *Frame Analysis Including Change of Geometry*, Proceedings of the ASCE, Journal of the Structural Division, Volume 94, pp.627-644, 1968

[18] **Cook R. D.**, *Finite Element Modelling for Stress Analysis*, John Wiley & Sons, Inc., 1994, ISBN 0-471-10774-3

[19] **Igusa T.**, *Critical Configurations of Systems Subjected to Wide-Band Input*, Journal of Sound and Vibration, Volume 168, No 3, pp.525-541, 1993